Available online at www.sciencedirect.com
SCIENCE DIRECT®
Journal of Sound and Vibration 265 (2003) 819–839
JOURNAL OF SOUND AND VIBRATION
www.elsevier.com/locate/jsvi

Finite-amplitude waves in isotropic elastic plates

W.J.N. de Lima, M.F. Hamilton*

Department of Mechanical Engineering, The University of Texas at Austin, Austin, TX 78712-1063, USA

Received 4 June 2001; accepted 10 August 2002

Abstract

The propagation of finite-amplitude waves in a homogeneous, isotropic, stress-free elastic plate is investigated theoretically. Geometric and weak material non-linearities are included, and perturbation is used to obtain solutions of the non-linear equations of motion for harmonic generation in the waveguide. Solutions for the second-harmonic, sum, and difference-frequency components are obtained via modal decomposition. Ordinary differential equations for the modal amplitudes in the expansion of the second-order solution are obtained using a reciprocity relation. There are no restrictions on the modes or frequencies of the primary waves. Two conditions for internal resonance are quantified: phase matching, and transfer of power from the primary to the secondary wave.

1. Introduction

Although non-linear elastic wave propagation is a subject of considerable interest [1], most of the research has focused on bulk [2] and surface waves [3,4]. Bulk and surface waves are non-dispersive, and therefore all frequency components propagate at the same speed. In contrast, waveguide modes are highly dispersive, and they can propagate in a wide variety of modes.

One important application of elastic waves is non-destructive evaluation. Traditional ultrasonic NDE is based on linear theory and normally relies on measuring some particular parameter (sound velocity, attenuation, transmission and reflection coefficients) of the propagating signal to determine the elastic properties of a material or to detect defects [5,6]. The presence of defects changes the phase and/or amplitude of the output signal, but the frequency of the input and output signals is the same. Linear waveguide modes have been used in non-destructive testing of large structures because these waves can propagate for long distances [5,7–10].

It is known that non-linear material parameters are much more sensitive to defects than are the linear parameters [11] and therefore non-linear elastic waves have been proposed as a potential

*Corresponding author. Tel.: 512-471-1131; fax: 512-471-8727.
E-mail address: hamilton@mail.utexas.edu (M.F. Hamilton).

0022-460X/03/$ - see front matter
doi:10.1016/S0022-460X(02)01260-9

tool for ultrasound NDE. The principal difference between linear and non-linear ultrasound NDE is that in the latter the existence and characteristics of defects are often related to an acoustic signal whose frequency differs from that of the input signal [12–18].

There are very few studies of guided non-linear elastic waves despite the focus in NDE on plates, rods and shells. Thin non-linear waveguides have been studied using approximate 1-D theories to describe the displacement vector. These approximate theories are valid only when the wavelength is large compared with the thickness of the waveguide. In this long wavelength (low frequency) regime the effect of dispersion is weak. Non-linearity and weak dispersion can result in the existence of stationary solutions (solitons) for this kind of problem [19].

An investigation of second-harmonic generation in isotropic plates has been reported recently by Deng [20–22]. In these papers, the primary and secondary fields are represented by pairs of plane waves that satisfy stress-free boundary conditions on the surfaces [23]. Only the case of resonant second-harmonic generation is considered, requiring the existence of a second-harmonic wave whose phase speed matches that of the primary wave. All non-resonant second-harmonic waves that are generated are ignored. In particular, contributions due to near-resonance conditions, for which significant second-harmonic generation can occur, are not taken into account. For example, the authors conclude that cumulative harmonic generation cannot occur in the lowest antisymmetric and symmetric modes. However, these are precisely the modes that support Rayleigh waves at high frequencies, which are well known to involve resonant harmonic generation and even shock formation (see, e.g., the literature review in Ref. [24]). More generally, because the analysis is not formulated in terms of waveguide modes, the development is cumbersome and interpretation of the results is obscured. Moreover, the formalism relies upon the rectangular symmetry of plates and is not applicable to geometries such as cylindrical rods and shells.

The present investigation is based on normal mode expansion of the secondary wave field. All modes of the secondary wave field are taken into account, not just those in resonance with the primary wave. The problem is formulated for isotropic elastic waveguides with constant but arbitrary cross-section. The non-linear equations of elasticity are solved by successive approximations. In the first approximation, the primary wave is described by linear theory. The secondary wave field is calculated by solving inhomogeneous but still linear equations of motion, in which the forcing function is determined by using the solution for the primary wave to evaluate the lowest order non-linear terms of the elasticity equations. The method described by Auld [23] for linear elastic waveguides subjected to body and surface forces is used to obtain the normal mode solution for the secondary waves. Second-harmonic, sum, and difference-frequency generation are considered. Calculations are presented for harmonic generation in plates. Results obtained for cylindrical rods [25] will be presented in a subsequent article.

2. Non-linear boundary value problem

The boundary value problem associated with non-linear elastic waves in a stress-free plate (Fig. 1), in Lagrangian coordinates, is given by the equation of motion

$$(\lambda + 2\mu)\nabla(\nabla \cdot \mathbf{u}) - \mu\nabla \times (\nabla \times \mathbf{u}) + \mathbf{f} = \rho_0 \frac{\partial^2 \mathbf{u}}{\partial t^2}, \tag{1}$$

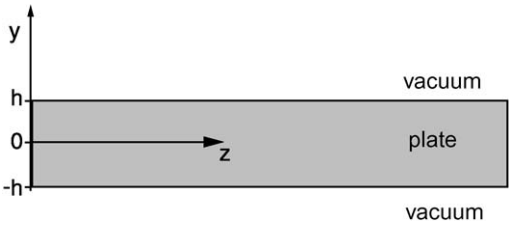

Fig. 1. Stress-free plate of thickness $2h$ in a vacuum. The plate is infinite in the x and z directions.

and the stress-free boundary condition

$$(\mathbf{S}^L - \bar{\mathbf{S}}) \cdot \mathbf{n}_y = \mathbf{0} \ \text{ on } \ \mathscr{S}, \tag{2}$$

where $\mathbf{u}$ is the particle displacement, λ and μ are the Lamé elastic constants, ρ_0 is the initial density of the body, $\mathbf{n}_y$ is a unit vector perpendicular to the surface $\mathscr{S}$ of the plate, $\mathbf{S}^L$ is the linear part of the first Piola–Kirchhoff stress tensor given in terms of the particle displacement as

$$\mathbf{S}^L(\mathbf{u}) = \frac{\lambda}{2}(\boldsymbol{\nabla}\mathbf{u} + \boldsymbol{\nabla}^{\mathrm{T}}\mathbf{u})\mathbf{I} + \mu(\boldsymbol{\nabla}\mathbf{u} + \boldsymbol{\nabla}^{\mathrm{T}}\mathbf{u}), \tag{3}$$

and $\bar{\mathbf{S}}$ and $\mathbf{f}$ collect all non-linear terms. The expressions for $\bar{\mathbf{S}}$ and $\mathbf{f}$ were derived by Gol'dberg [26] and are given by

$$\begin{aligned}\bar{S}_{ij} = {} & \left(\frac{\lambda}{2}\frac{\partial u_k}{\partial x_l}\frac{\partial u_k}{\partial x_l} + \mathscr{C}\frac{\partial u_k}{\partial x_k}\frac{\partial u_l}{\partial x_l}\right)\delta_{ij} + \mathscr{B}\frac{\partial u_k}{\partial x_k}\frac{\partial u_j}{\partial x_i} + \frac{\mathscr{A}}{4}\frac{\partial u_j}{\partial x_k}\frac{\partial u_k}{\partial x_i} \\ & + \frac{\mathscr{B}}{2}\left(\frac{\partial u_k}{\partial x_l}\frac{\partial u_k}{\partial x_l} + \frac{\partial u_k}{\partial x_l}\frac{\partial u_l}{\partial x_k}\right)\delta_{ij} + (\lambda + \mathscr{B})\frac{\partial u_k}{\partial x_k}\frac{\partial u_i}{\partial x_j} \\ & + \left(\mu + \frac{\mathscr{A}}{4}\right)\left(\frac{\partial u_i}{\partial x_k}\frac{\partial u_j}{\partial x_k} + \frac{\partial u_k}{\partial x_i}\frac{\partial u_k}{\partial x_j} + \frac{\partial u_i}{\partial x_k}\frac{\partial u_k}{\partial x_j}\right) + O(u_i^3),\end{aligned} \tag{4}$$

$$\begin{aligned}f_i = {} & \left(\mu + \frac{\mathscr{A}}{4}\right)\left(\frac{\partial^2 u_l}{\partial x_k^2}\frac{\partial u_l}{\partial x_i} + \frac{\partial^2 u_l}{\partial x_k^2}\frac{\partial u_i}{\partial x_l} + 2\frac{\partial^2 u_i}{\partial x_l \partial x_k}\frac{\partial u_l}{\partial x_k}\right) \\ & + \left(\lambda + \mu + \frac{\mathscr{A}}{4} + \mathscr{B}\right)\left(\frac{\partial^2 u_l}{\partial x_i \partial x_k}\frac{\partial u_l}{\partial x_k} + \frac{\partial^2 u_k}{\partial x_l \partial x_k}\frac{\partial u_i}{\partial x_l}\right) \\ & + (\lambda + \mathscr{B})\left(\frac{\partial^2 u_i}{\partial x_k^2}\frac{\partial u_l}{\partial x_l}\right) + \left(\frac{\mathscr{A}}{4} + \mathscr{B}\right)\left(\frac{\partial^2 u_k}{\partial x_l \partial x_k}\frac{\partial u_l}{\partial x_i} + \frac{\partial^2 u_k}{\partial x_i \partial x_k}\frac{\partial u_k}{\partial x_l}\right) \\ & + (\mathscr{B} + 2\mathscr{C})\left(\frac{\partial^2 u_k}{\partial x_i \partial x_k}\frac{\partial u_l}{\partial x_l}\right) + O(u_i^3).\end{aligned} \tag{5}$$

Gol'dberg considered the medium to be hyperelastic and used the expression for the strain energy $\mathscr{E}$ proposed by Landau and Lifshitz [27],

$$\mathscr{E} = \tfrac{1}{2}\lambda I_1^2 + \mu I_2 + \tfrac{1}{3}\mathscr{C} I_1^3 + \mathscr{B} I_1 I_2 + \tfrac{1}{3}\mathscr{A} I_3 + O(E_{ij}^4), \tag{6}$$

where $I_1 = E_{ii}, I_2 = E_{ij}E_{ji}$, and $I_3 = E_{ij}E_{jk}E_{ki}$ are invariants of the Lagrangian strain tensor E_{ij}, and $\mathscr{A}$, $\mathscr{B}$ and $\mathscr{C}$ are the third-order elastic constants [27].

We shall solve the non-linear boundary value problem [Eqs. (1) and (2)] via simple perturbation, which is based on writing the solution as a sum of two terms,

$$\mathbf{u} = \mathbf{u}^{(1)} + \mathbf{u}^{(2)}, \tag{7}$$

where $\mathbf{u}^{(1)}$ is the primary solution and $\mathbf{u}^{(2)}$ is the secondary solution. The solution $\mathbf{u}^{(2)}$ is a perturbation due to non-linearity, and it is assumed to be small compared to $\mathbf{u}^{(1)}$:

$$|\mathbf{u}^{(2)}| \ll |\mathbf{u}^{(1)}|. \tag{8}$$

We shall refer to Eq. (8) as the perturbation condition. After substituting Eq. (7) into Eqs. (1) and (2), we divide the non-linear boundary value problem into two linear boundary value problems, namely, the first and second order approximations of the non-linear boundary value problem. In the first order approximation we have

$$(\lambda + 2\mu)\boldsymbol{\nabla}(\boldsymbol{\nabla} \cdot \mathbf{u}^{(1)}) - \mu\boldsymbol{\nabla} \times (\boldsymbol{\nabla} \times \mathbf{u}^{(1)}) - \rho_0 \frac{\partial^2 \mathbf{u}^{(1)}}{\partial t^2} = \mathbf{0}, \tag{9}$$

$$\mathbf{S}^L(\mathbf{u}^{(1)}) \cdot \mathbf{n}_y = \mathbf{0} \ \text{ on } \ \mathscr{S}, \tag{10}$$

where on $\mathbf{S}^L(\mathbf{u}^{(1)})$ is the first-order approximation of the first Piola–Kirchhoff stress tensor given in terms of $\mathbf{u}^{(1)}$. At second order we have

$$(\lambda + 2\mu)\boldsymbol{\nabla}(\boldsymbol{\nabla} \cdot \mathbf{u}^{(2)}) - \mu\boldsymbol{\nabla} \times (\boldsymbol{\nabla} \times \mathbf{u}^{(2)}) - \rho_0 \frac{\partial^2 \mathbf{u}^{(2)}}{\partial t^2} = -\mathbf{f}^{(1,1)}, \tag{11}$$

$$\mathbf{S}^L(\mathbf{u}^{(2)}) \cdot \mathbf{n}_y = -\bar{\mathbf{S}}^{(1,1)} \cdot \mathbf{n}_y \ \text{ on } \ \mathscr{S}, \tag{12}$$

where $\mathbf{S}^L(\mathbf{u}^{(2)})$ is the second order approximation of the first Piola–Kirchhoff stress tensor, and where $\mathbf{f}^{(1,1)}$ and $\bar{\mathbf{S}}^{(1,1)}$ contain quadratic terms in $\mathbf{u}^{(1)}$. Eq. (8) permits us to disregard the products of $\mathbf{u}^{(1)}$ and $\mathbf{u}^{(2)}$ and the quadratic terms in $\mathbf{u}^{(2)}$, which are of third and fourth order, respectively.

The solution of the first order problem, Eqs. (9) and (10), is identified as the primary wave field, and these are the plate modes. When the solution $\mathbf{u}^{(1)}$ is known, the terms $\mathbf{f}^{(1,1)}$ and $\bar{\mathbf{S}}^{(1,1)}$ are determined, and they are the forcing functions on the right sides of Eqs. (11) and (12). We obtain $\bar{\mathbf{S}}^{(1,1)}$ and $\mathbf{f}^{(1,1)}$ by substituting $\mathbf{u}^{(1)}$ into Eqs. (4) and (5). The solution $\mathbf{u}^{(2)}$ can be interpreted as a solution of a forced linear waveguide with an external force applied in the volume, $\mathbf{f}^{(1,1)}$, and on the boundary, $\bar{\mathbf{S}}^{(1,1)} \cdot \mathbf{n}_y$. Modal expansion and a reciprocity relation are used in Section 4 to obtain the solution $\mathbf{u}^{(2)}$.

3. Plate modes

An individual plate mode $\mathbf{u}^{(1)}$ can be written in the form [23,28]

$$\mathbf{u}^{(1)}(y, z, t) = \mathbf{u}^{(1)}(y)\mathrm{e}^{\mathrm{i}(\kappa z - \omega t)}, \tag{13}$$

where ω is the frequency and κ is the propagation wavenumber. Four different families of modes can propagate: the symmetric and antisymmetric Rayleigh–Lamb modes (RL modes), and the symmetric and antisymmetric horizontally polarized shear modes (SH modes). The particle

displacement $\mathbf{u}^{(1)}(y)$ corresponding to these modes can be written as follows [28]:

$$u_x^{(1)} = C\sin\beta y + D\cos\beta y, \tag{14}$$

$$u_y^{(1)} = -\alpha A\sin\alpha y - \kappa H\sin\beta y - \alpha B\cos\alpha y + \mathrm{i}\kappa G\cos\beta y, \tag{15}$$

$$u_z^{(1)} = \mathrm{i}\kappa A\cos\alpha y + \beta H\cos\beta y + \mathrm{i}\kappa B\sin\alpha y - \beta G\sin\beta y, \tag{16}$$

with $A, B, D, G, H = 0$ and $C \neq 0$ for antisymmetric SH modes, $A, B, C, G, H = 0$ and $D \neq 0$ for symmetric SH modes, A, $H \neq 0$ and $B, C, D, G = 0$ for symmetric RL modes; and $A, C, D, H = 0$ and $B, G \neq 0$ for antisymmetric RL modes. The dispersion equation for the SH modes is

$$(\omega h/c_t)^2 = (n\pi/2)^2 + (\kappa h)^2 \quad \begin{cases} n = 0, 2, 4, 6, \ldots & \text{symmetric,} \\ n = 1, 3, 5, 7, \ldots & \text{antisymmetric} \end{cases} \tag{17}$$

and for the RL modes it is

$$\frac{\tan\beta h}{\tan\alpha h} = -\left[\frac{(\kappa^2 - \beta^2)^2}{4\alpha\beta\kappa^2}\right]^{\pm 1} \quad \begin{cases} +1, & \text{symmetric,} \\ -1, & \text{antisymmetric,} \end{cases} \tag{18}$$

where

$$\alpha = \sqrt{(\omega/c_l)^2 - \kappa^2}, \quad \beta = \sqrt{(w/ct)^2 - \kappa^2}, \tag{19}$$

$c_l = \sqrt{(\lambda + 2\mu)/\rho_0}$ is the longitudinal wave speed, and $c_t = \sqrt{\mu/\rho_0}$ is the transverse wave speed.

For a given ω there exists a finite number of propagating modes (κ a real number) and an infinite number of evanescent modes (κ a complex or pure imaginary number), and the evanescent modes appear in complex conjugate pairs, i.e., for a given frequency ω, if the pair (ω, κ) is a solution of the dispersion equation, then (ω, κ^*) is also a solution [23,29]. This is relevant in the solution of the non-linear problem because, in Section 4.1, these modes are used in the expansion of the second order velocity field. The dispersion curves for propagating SH and RL modes of an aluminum plate are shown in Figs. 2 and 3, respectively, in terms the following dimensionless angular frequency $\bar{\omega}$ and wavenumber $\bar{\kappa}$:

$$\bar{\omega} = 2h\omega/\pi c_t, \quad \bar{\kappa} = 2h\kappa/\pi. \tag{20}$$

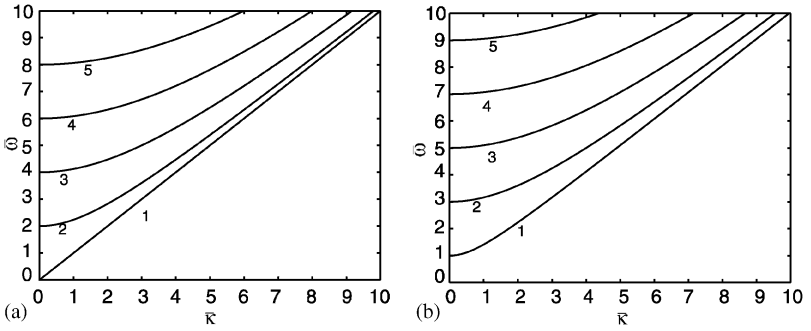

Fig. 2. Dispersion curves for SH modes of an aluminum plate: (a) symmetric modes and (b) antisymmetric modes.

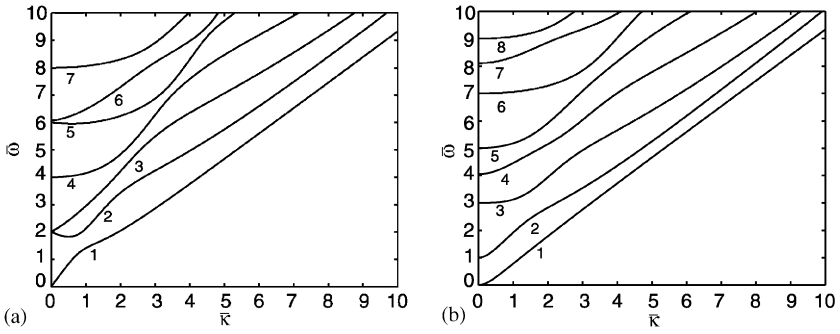

Fig. 3. Dispersion curves for RL modes of an aluminum plate: (a) symmetric modes and (b) antisymmetric modes.

Table 1
Physical properties

Material	ρ_0 (kg/m^3)	c_l (m/s)	c_t (m/s)	λ (GPa)	μ (GPa)	$\mathscr{A}$ (GPa)	$\mathscr{B}$ (GPa)	$\mathscr{C}$ (GPa)
Aluminum	2727[a]	6381[a]	3150[a]	57[b]	27[b]	−320[c]	−200[c]	−190[c]

[a] Landsberger [31].
[b] Kinsler et al. [32].
[c] Landolt-Bornstein [33].

The elastic moduli for aluminum, for both linear and non-linear propagation, are provided in Table 1.

4. Harmonic generation

In this section we develop the solution for the second-order problem, Eqs. (11) and (12). We introduce the notation

$$\mathbf{S}^{(j)} \equiv \mathbf{S}^{L}(\mathbf{u}^{(j)}), \quad j = 1, 2. \tag{21}$$

Now note that Eqs. (11) and (12) may also be obtained from the set of equations

$$\boldsymbol{\nabla} \cdot \mathbf{S}^{(2)} + \mathbf{f}^{(1,1)} = \rho_0 \frac{\partial^2 \mathbf{u}^{(2)}}{\partial t^2}, \tag{22}$$

$$\mathbf{e}^{(2)} = \tfrac{1}{2}(\boldsymbol{\nabla}\mathbf{u}^{(2)} + \boldsymbol{\nabla}^{\mathrm{T}}\mathbf{u}^{(2)}), \tag{23}$$

$$\mathbf{S}^{(2)} = (\lambda + \mu)\mathbf{e}^{(2)}\mathbf{I} + \mu\mathbf{e}^{(2)}, \tag{24}$$

$$\mathbf{S}^{(2)} \cdot \mathbf{n}_y = -\bar{\mathbf{S}}^{(1,1)} \cdot \mathbf{n}_y, \quad \text{on } \mathscr{S}, \tag{25}$$

by substituting Eq. (23) into Eq. (24) and the result into Eq. (22). From Eqs. (22)–(25), we can thus interpret the secondary solution as the linear solution of a forced waveguide with stress

tensor $\mathbf{S}^{(2)}$, strain tensor $\mathbf{e}^{(2)}$, external force applied in the volume, $\mathbf{f}^{(1,1)}$, and traction applied on the boundary, $\bar{\mathbf{t}} = -\bar{\mathbf{S}}^{(1,1)} \cdot \mathbf{n}_y$. In Section 4.1 a formalism is introduced for constructing the second order solution using modal expansion. The formalism is given by Auld [23] for an elastic plate waveguide. In this formalism, a reciprocity relation is obtained through algebraic manipulations of the field equations (22)–(25). The reciprocity relation is used to prove orthogonality of the plate modes. A solution in terms of the particle velocity is expressed as a linear combination of the modes. Then, the reciprocity and orthogonality relations are used to obtain the amplitude coefficients in the modal expansion. One advantage of this approach is that each mode individually satisfies both the source condition at $z = 0$ and the boundary condition along the surfaces of the plate. The approach is also appealing because of the physical insight provided by interpreting the excitation by the primary wave as external surface and volume forces.

In subsequent sections we assume that a source excites either one or two plate modes at $z = 0$. The leading solution $\mathbf{u}^{(1)}$ is thus determined, and we investigate how these excited modes interact with each other and with the medium by finding the secondary solution $\mathbf{u}^{(2)}$.

4.1. Second-order solution

Consider two propagating plate modes with frequencies ω_a and ω_b, and corresponding wavenumbers κ_a and κ_b, that are excited at $z = 0$. The primary solution thus has the form

$$\mathbf{u}^{(1)} = \tfrac{1}{2}\mathbf{u}^a(y)\mathrm{e}^{\mathrm{i}(\kappa_a z - \omega_a t)} + \tfrac{1}{2}\mathbf{u}^b(y)\mathrm{e}^{\mathrm{i}(\kappa_b z - \omega_b t)} + \text{c.c.}, \tag{26}$$

where c.c. stands for complex conjugate. Substituting Eq. (26) in the expressions for $\mathbf{f}^{(1,1)}$ and $\bar{\mathbf{S}}^{(1,1)}$, we may write

$$\begin{aligned}\mathbf{f}^{(1,1)} = {} & \bar{\mathbf{f}}^{2\omega_a}(y)\mathrm{e}^{\mathrm{i}2(\kappa_a z - \omega_a t)} + \bar{\mathbf{f}}^{2\omega_b}(y)\mathrm{e}^{\mathrm{i}2(\kappa_b z - \omega_b t)} \\ & + \bar{\mathbf{f}}^{+}(y)\mathrm{e}^{\mathrm{i}[(\kappa_a + \kappa_b)z - \omega_+ t]} + \bar{\mathbf{f}}^{-}(y)\mathrm{e}^{\mathrm{i}[(\kappa_a - \kappa_b)z - \omega_- t]} + \text{c.c.},\end{aligned} \tag{27}$$

$$\begin{aligned}\bar{\mathbf{S}}^{(1,1)} = {} & \bar{\mathbf{S}}^{2\omega_a}(y)\mathrm{e}^{\mathrm{i}2(\kappa_a z - \omega_a t)} + \bar{\mathbf{S}}^{2\omega_b}(y)\mathrm{e}^{\mathrm{i}2(\kappa_b z - \omega_b t)} \\ & + \bar{\mathbf{S}}^{+}(y)\mathrm{e}^{\mathrm{i}[(\kappa_a + \kappa_b)z - \omega_+ t)]} + \bar{\mathbf{S}}^{-}(y)\mathrm{e}^{\mathrm{i}[(\kappa_a - \kappa_b)z - \omega_- t)]} + \text{c.c.},\end{aligned} \tag{28}$$

where $\omega_\pm = \omega_a \pm \omega_b$ ($\omega_a > \omega_b$ is assumed), $\bar{\mathbf{f}}^{2\omega_a}$ and $\bar{\mathbf{S}}^{2\omega_a}$ are due to the self-interaction of the excited mode $\mathbf{u}^a(y)$, $\bar{\mathbf{f}}^{2\omega_b}$ and $\bar{\mathbf{S}}^{2\omega_b}$ are due to the self-interaction of the excited mode $\mathbf{u}^b(y)$, and $\bar{\mathbf{f}}^{+}, \bar{\mathbf{S}}^{+}, \bar{\mathbf{f}}^{-}$ and $\bar{\mathbf{S}}^{-}$ are due to the mutual interaction of $\mathbf{u}^a(y)$ with $\mathbf{u}^b(y)$. The expressions for $\bar{\mathbf{f}}^{2\omega_a}, \bar{\mathbf{S}}^{2\omega_a}, \bar{\mathbf{f}}^{2\omega_b}, \bar{\mathbf{S}}^{2\omega_b}, \bar{\mathbf{f}}^{+}, \bar{\mathbf{S}}^{+}, \bar{\mathbf{f}}^{-}$ and $\bar{\mathbf{S}}^{-}$ are extremely lengthy for any mode $\mathbf{u}^a$ and $\mathbf{u}^b$, and hence they will not be presented here. The terms with time dependencies $\mathrm{e}^{-\mathrm{i}\omega_- \mathrm{t}}$ and $\mathrm{e}^{-\mathrm{i}\omega_+ \mathrm{t}}$ are the difference and sum frequency components, respectively, and the terms with time dependencies $\mathrm{e}^{-\mathrm{i}2\omega_a t}$ and $\mathrm{e}^{-\mathrm{i}2\omega_b t}$ are the second-harmonic components.

The secondary solution can be obtained separately, because the second-order problem is linear. To simplify the notation, we rewrite Eqs. (27) and (28) in the form

$$\mathbf{f}^{(1,1)} = \bar{\mathbf{f}}^{\pm}(y)\mathrm{e}^{\mathrm{i}[(\kappa_\mathrm{a} \pm \kappa_b)z - \omega_\pm t]} + \text{c.c.}, \tag{29}$$

$$\bar{\mathbf{S}}^{(1,1)} = \bar{\mathbf{S}}^{\pm}(y)\mathrm{e}^{\mathrm{i}[(\kappa_\mathrm{a} \pm \kappa_b)z - \omega_\pm t]} + \text{c.c.} \tag{30}$$

Second-harmonic generation is considered as a special case of sum frequency generation, in which only a single mode is excited [$\mathbf{u}^b(y) = \mathbf{0}$ and $\mathbf{u}^a(y) \neq \mathbf{0}$].

Following Auld [23], we write the secondary solution as a linear combination of the waveguide modes at frequency $\omega_\pm$:

$$\mathbf{v}^{(2)}(y,z,t) = \frac{1}{2}\sum_{m=1}^{\infty} A_m(z)\mathbf{v}_m(y)\mathrm{e}^{-\mathrm{i}\omega_\pm t} + \text{c.c.}, \tag{31}$$

$$\mathbf{S}^{(2)}(y,z,t)\cdot\mathbf{n}_z = \frac{1}{2}\sum_{m=1}^{\infty} A_m(z)\mathbf{S}_m(y)\cdot\mathbf{n}_z\mathrm{e}^{-\mathrm{i}\omega_\pm t} + \text{c.c.}, \tag{32}$$

where $\mathbf{v}^{(2)} = \partial\mathbf{u}^{(2)}/\partial t, \mathbf{v}_m$ is the particle velocity of the mth mode at frequency $\omega_\pm$, $\mathbf{S}_m$ is a tensor related to $\mathbf{v}_m$ through Eqs. (23) and (24), and A_m is the second order modal amplitude to be determined. As shown by Auld [23], A_m is the solution of the following ordinary differential equation to be solved for each individual value of m:

$$4\mathscr{P}_{mn}\left(\frac{\mathrm{d}}{\mathrm{d}z} - \mathrm{i}\kappa_n^*\right)A_m(z) = (f_n^{surf} + f_n^{vol})\mathrm{e}^{\mathrm{i}(\kappa_a \pm \kappa_b)z}, \quad m = 1,2,\ldots, \tag{33}$$

where

$$\mathscr{P}_{mn} = -\frac{1}{4}\int_{-h}^{h}\left(\frac{\mathbf{v}_n^*}{2}\cdot\frac{\mathbf{S}_m}{2} + \frac{\mathbf{v}_m}{2}\cdot\frac{\mathbf{S}_n^*}{2}\right)\cdot\mathbf{n}_z\,\mathrm{d}\Omega, \tag{34}$$

$$f_n^{surf} = -\tfrac{1}{2}\mathbf{v}_n^*\bar{\mathbf{S}}^{\pm}\cdot\mathbf{n}_y\big|_{y=-h}^{y=h}, \tag{35}$$

$$f_n^{vol} = \frac{1}{2}\int_{-h}^{h}\bar{\mathbf{f}}^{\pm}\cdot\mathbf{v}_n^*\,\mathrm{d}y, \tag{36}$$

and κ_n is the wavenumber of the mode identified by index n that is not orthogonal ($\mathscr{P}_{mn} \neq 0$) to the mode with wavenumber κ_m. Note that in Eq. (33) there is no summation over m. The orthogonality relation for propagating and evanescent modes is given by [23]

$$\mathscr{P}_{mn} = 0, \quad \kappa_m \neq \kappa_n^*. \tag{37}$$

According to Eq. (37), a propagating mode m is orthogonal to all modes except itself, an evanescent mode m is orthogonal to itself and for any given evanescent mode m there is only one evanescent mode n that is not orthogonal to mode m. Hence, for each mode m there is always a single mode n to be used in Eq. (33). Note that we introduced the factor of $\frac{1}{2}$ and the complex conjugate in Eqs. (26) and (31), unlike in the equation presented by Auld [23]. The reason for doing so here is that when evaluating products of solutions it is essential that real functions are used. This problem does not arise in the linear theory. We have therefore shown explicitly when the factors of 2 appear in Eqs. (34)–(36) to facilitate comparison with the equations presented by Auld [23].

From the source condition, Eq. (38), we have

$$\mathbf{v}^{(2)}(y,0,t) = \mathbf{0} \tag{38}$$

and consequently from Eq. (31) we have at second order the following initial condition for each modal amplitude:

$$A_m(0) = 0. \tag{39}$$

Hence, Eq. (33) has the solution

$$A_m(z) = \bar{A}_m(z)\mathrm{e}^{\mathrm{i}(\kappa_a \pm \kappa_b)z} - \bar{A}_m(0)\mathrm{e}^{\mathrm{i}\kappa_n^* z}, \tag{40}$$

where

$$\bar{A}_m(z) = \frac{\mathrm{i}(f_n^{vol} + f_n^{surf})}{4\mathscr{P}_{mn}[\kappa_n^* - (\kappa_a \pm \kappa_b)]}, \quad \kappa_n^* \neq \kappa_a \pm \kappa_b, \tag{41}$$

$$\bar{A}_m(z) = \left(\frac{f_n^{vol} + f_n^{surf}}{4\mathscr{P}_{mn}}\right) z, \quad \kappa_n^* = \kappa_a \pm \kappa_b. \tag{42}$$

From Eqs. (35) and (39), we observe that the boundary and source conditions are satisfied for each mode used in the expansion, Eq. (31).

For propagating modes, $\mathscr{P}_{mm}$ is the complex power flux in direction $\mathbf{n}_z$ of the mth propagating mode used in the expansion of the secondary solution given in Eq. (31). Also, f_m^{vol} and f_m^{surf} are interpreted as the power flux through the volume and through the surface, respectively, due to the primary wave.

When $\kappa_n^* \neq \kappa_a \pm \kappa_b$, the amplitude of the secondary solution remains bounded and oscillates with a spatial periodicity, often called the dispersion length L_n, given by

$$L_n = \frac{2\pi}{|\kappa_n^* - (\kappa_a \pm \kappa_b)|}. \tag{43}$$

When phase matching (also called synchronism) occurs between the primary wave and one of the waveguide modes used in the expansion of the secondary solution, i.e., $\kappa_n^* = \kappa_a \pm \kappa_b$ or $L_n \to \infty$, and if the power flux due to the primary solution is different from zero ($f_n^{vol} + f_n^{surf} \neq 0$), the amplitude of the secondary solution grows linearly in the direction of propagation. This phenomenon is called internal resonance [30]. Hence, two conditions for internal resonance must be satisfied: (1) synchronism, or phase matching, $\kappa_n^* = \kappa_a \pm \kappa_b$; (2) non-zero power flux, $f_n^{vol} + f_n^{surf} \neq 0$.

In order to illustrate what we mean by synchronism we plot the dispersion curves for a certain waveguide (Fig. 4), and choose the two modes (ω_a, κ_a) and (ω_b, κ_b) as the primary waves. If one of the components of the forcing function $\mathbf{f}^{(1,1)}$, say the difference frequency ω_-, coincides with one of the modes used in the expansion of the secondary solution, phase matching occurs, i.e., this component propagates at the same phase speed, and is thus in synchronism with, the forcing functions. In Fig. 4(a) we present an example with phase matching. In this figure the difference-frequency component can propagate in a mode for which $\kappa_1 = \kappa_a - \kappa_b$, and there is synchronism. In Fig. 4(b) an example without phase matching is presented. Here, the only two modes in which the difference frequency can propagate have wavenumbers different from that of the forcing functions ($\kappa_1, \kappa_2 \neq \kappa_a - \kappa_b$), and the interaction is asynchronous.

No evanescent modes can be in resonance with primary waves that consist only of propagating modes. Hence, evanescent modes contribute to the expansion only as bounded oscillations.

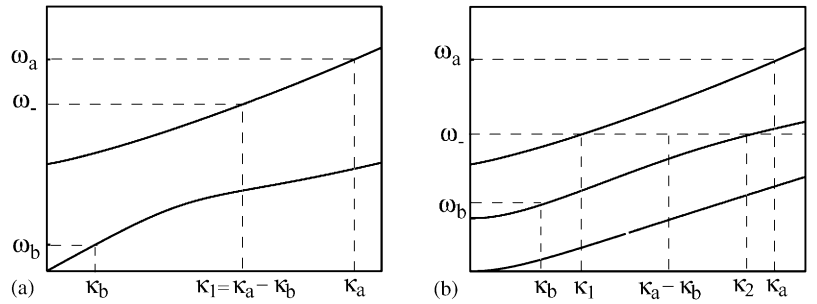

Fig. 4. Cases of (a) synchronous and (b) asynchronous interaction of the primary waves with the difference-frequency component, corresponding to whether the point $(\omega_-, \kappa_a - \kappa_b)$ does or does not lie on a dispersion curve, respectively.

Now suppose that a propagating mode, say the rth mode with wavenumber κ_r, is in resonance with the primary wave. The secondary solution then has the form

$$\mathbf{v}^{(2)} = \frac{1}{2}\sum_{m\neq r}[A_m(z)\mathbf{v}_m e^{-i\omega_\pm t}] + \frac{z}{2} f_r \mathbf{v}_r e^{i(\kappa_r z - \omega_\pm t)} + \text{c.c.}, \tag{44}$$

where

$$f_r = \frac{f_r^{vol} + f_r^{surf}}{4\mathscr{P}_{rr}} \tag{45}$$

and A_m $(m\neq r)$ is given by Eqs. (40) and (41). Since the summation in Eq. (44) is bounded, as z increases the second term eventually dominates the first, and the secondary solution can be expressed as

$$\mathbf{v}^{(2)} = \frac{z}{2} f_r \mathbf{v}_r e^{i(\kappa_r z - \omega_\pm t)} + \text{c.c.} \tag{46}$$

In the absence of internal resonance, all modes are needed to represent the secondary solution. However, when one mode is in resonance with the primary wave, this mode is the dominant term in the solution, and the other terms can be neglected after a certain propagation distance z_1, where z_1 is defined as the propagation distance where the amplitude of the bounded term equals that of the resonant term in Eq. (44):

$$\left|\sum_{m\neq r} A_m \mathbf{v}_m\right| = z_1 |f_r \mathbf{v}_r|. \tag{47}$$

In addition, the perturbation condition, Eq. (8) must be satisfied, and therefore the solution given by Eq. (46) is valid in the interval

$$z_1 < z < z_2, \tag{48}$$

where

$$z_2 = |\mathbf{u}^{(1)}|/|f_r \mathbf{u}_r| \tag{49}$$

and $\mathbf{u}_r$ is the particle displacement of the rth mode at frequency $\omega_\pm$.

The evanescent modes are important in Eq. (44) to guarantee an infinite number of modes in the expansion. However, since these modes do not propagate and are important only close to the source [23], they will not be used to estimate z_1 and z_2.

In the next sections we present examples based on Eqs. (27)–(36) for longitudinal plane waves and infinite plates. The medium considered is aluminum, whose elastic constants are given in Table 1.

4.2. Longitudinal plane waves

In order to facilitate the understanding of the more difficult calculations associated with waveguide problems presented in the following sections, we first consider the solution for second-harmonic generation by a longitudinal plane wave in an unbounded medium. For a longitudinal plane wave propagating in the z direction, Eq. (1) becomes [26]

$$(\lambda + 2\mu)\frac{\partial^2 u_z}{\partial z^2} - \rho_0 \frac{\partial^2 u_z}{\partial t^2} - \gamma \frac{\partial u_z}{\partial z}\frac{\partial^2 u_z}{\partial z^2} = 0, \tag{50}$$

where

$$\gamma = 3(\lambda + 2\mu) + 2\mathscr{A} + 6\mathscr{B} + 2\mathscr{C} \tag{51}$$

is a coefficient of non-linearity. To simplify the notation we replace u_z with u for the rest of this section. The linear solution is the plane wave

$$u^{(1)} = \tfrac{1}{2}U_0 e^{i(\kappa_a z - \omega_a t)} + \text{c.c.} = U_0 \cos(\kappa_a z - \omega_a t). \tag{52}$$

For the secondary wave we have

$$(\lambda + 2\mu)\frac{\partial^2 u^{(2)}}{\partial z^2} - \rho_0 \frac{\partial^2 u^{(2)}}{\partial t^2} + f^{(1,1)} = 0, \tag{53}$$

where $f^{(1,1)}$ is given by

$$f^{(1,1)} = -\gamma \frac{\partial u^{(1)}}{\partial z}\frac{\partial^2 u^{(1)}}{\partial z^2}. \tag{54}$$

The source condition is

$$u^{(2)}(0, t) = 0. \tag{55}$$

Substituting Eq. (52) into Eq. (54) we obtain

$$f^{(1,1)} = \frac{i\gamma\kappa_a^3 U_0^2}{4} e^{i2(\kappa_a z - \omega_a t)} + \text{c.c.} \tag{56}$$

In order to solve Eq. (53) using the method outlined in Section 4.1, the reader may think of the unbounded medium as a plate with infinite width and with dispersion relation given by $\omega_a = c_l \kappa_a$. The solution for the particle velocity at frequency $2\omega_a$ is

$$v_1^{(2)}(z, t) = \tfrac{1}{2}v_1 e^{i2(\kappa_a z - \omega_a t)} + \text{c.c.}, \tag{57}$$

where subscript 1 means that there is only one mode at frequency $2\omega_a$. The stress tensor in Eq. (24) associated with longitudinal waves at frequency $2\omega_a$ reduces to

$$S_1^{(2)} = -\tfrac{1}{2}\rho_0 c_l v_1 e^{i2(\kappa_a z - \omega_a t)} + \text{c.c.} \tag{58}$$

Therefore, the expansion in Eq. (31) becomes

$$v^{(2)} = \tfrac{1}{2}A_1(z)v_1 e^{-i2\omega_a t} + \text{c.c.}, \tag{59}$$

where the amplitude $A_1(z)$ is given by

$$A_1(z) = \left(\frac{f_1^{vol} + f_1^{surf}}{4\mathscr{P}_{11}}\right) z e^{i2\kappa_a z}. \tag{60}$$

We now find the terms f_1^{vol}, f_1^{surf} and $\mathscr{P}_{11}$. Since the medium is unbounded we have $f_1^{surf} \equiv 0$. According to Eq. (34), the complex power $\mathscr{P}_{11}$ per unit volume is

$$\mathscr{P}_{11} = -\tfrac{1}{8}v_1 S_1 = \tfrac{1}{8}\rho_0 c_l v_1^2 \tag{61}$$

and according to Eq. (36) the power transfer from the primary wave through the volume is

$$f_1^{vol} = \frac{i\gamma\kappa_a^3 U_0^2}{8} v_1. \tag{62}$$

Substituting Eqs. (61) and (62) into Eq. (60) we obtain

$$A_1(z) = -\frac{i\gamma\kappa_a^3 U_0^2}{4\rho_0 c_l v_1} z e^{i2\kappa_a z} \tag{63}$$

and substituting Eq. (63) into Eq. (59) we have for the second-harmonic particle velocity

$$v^{(2)} = \tfrac{1}{2} f_r z e^{i2(\kappa_a z - \omega_a t)} + \text{c.c.}, \tag{64}$$

where

$$f_r = -\frac{i\gamma\kappa_a^3 U_0^2}{4\rho_0 c_l}. \tag{65}$$

For the second-harmonic particle displacement we have, from Eq. (59),

$$u^{(2)} = \frac{1}{16}\frac{\gamma\kappa_a^3 U_0^2}{\rho_0 c_l \omega_a} z e^{i2(\kappa_a z - \omega_a t)} + \text{c.c.} \tag{66}$$

By defining $\beta_l = \gamma/2\rho_0 c_l^2$ we thus recover the form presented by Norris [2]:

$$u^{(2)} = \frac{\beta_l}{4}\left(\frac{U_0\omega_a}{c_l}\right)^2 z \cos[2(\kappa_a z - \omega_a t)]. \tag{67}$$

Since we have only one mode in the expansion then $z_1 = 0$, and z_2 is found by equating the primary and secondary solutions as follows:

$$\frac{|u^{(2)}|}{|u^{(1)}|} = \frac{\beta_l}{4}\left(\frac{\omega_a}{c_l}\right)^2 U_0 z_2 \equiv 1. \tag{68}$$

Therefore $z_2 = 4c_l^2/\beta_l\omega_a^2 U_0$, and the solution in Eq. (67) is valid for

$$z \ll \frac{4c_l^2}{\beta_l\omega_a^2 U_0}. \tag{69}$$

4.3. Infinite plate

For an infinite plate with stress-free surface (see Fig. 1) the particle displacements of the primary waves are the plate modes presented in Section 3, which can be written in the form of Eq. (26). The expressions for $\mathbf{u}_a(y)$ and $\mathbf{u}_b(y)$ depend on which modes are excited. The dimensionless particle displacement $\bar{\mathbf{u}}$ and dimensionless mode amplitude $\bar{A}(z)$ used in the examples are defined as

$$\bar{\mathbf{u}} = \pi\mathbf{u}/2h, \quad \bar{A}_m(z) = \pi A_m(z)/2h. \tag{70}$$

4.3.1. Example 1: second harmonic, no resonance

In this first example, a monofrequency source at dimensionless frequency $\bar{\omega}_a = 1.4$ [see Eq. (20)] excites the first symmetric RL mode, for which $\bar{\kappa}_a = 0.994$. This mode is plotted in Fig. 5. From the dispersion equation [Eq. (18)] we find that eight propagating modes exist at the second-harmonic frequency. These are the modes used in the expansion of the second-harmonic component ($2\bar{\omega}_a = 2.8$, $2\bar{\kappa}_a = 1.988$). The dimensionless wavenumbers $\bar{\kappa}_m$ of these eight propagating modes are presented in Table 2.

Note that two modes in Table 2, the second antisymmetric RL mode and the second symmetric SH mode, are in phase with the primary wave, i.e., $\bar{\kappa}_m(2\bar{\omega}_a) = 2\bar{\kappa}_a(\bar{\omega}_a) = 1.988$. However, the power flux from the primary wave to these modes is zero ($f_m^{vol} + f_m^{surf} = 0$), and hence the amplitudes of these modes in the expansion are zero.

The reason for zero power flux from the primary wave to the symmetric SH mode lies in the fact that since the displacement vector of the symmetric RL mode has a zero u_x component and the other components are functions only of y, the x components of the vectors $\bar{\mathbf{f}}^{2\omega_a}$ and $\bar{\mathbf{S}}^{2\omega_a} \cdot \mathbf{n}_y$ are zero, and therefore the terms in Eqs. (35) and (36) for the SH modes ($v_x \neq 0, v_y, v_z = 0$) are zero.

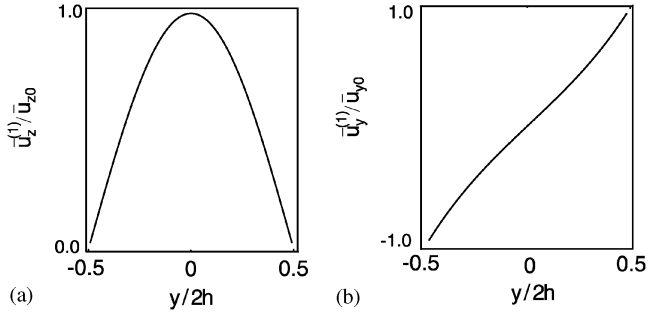

Fig. 5. Primary wave—first symmetric RL mode shape for $\bar{\omega}_a = 1.41$: (a) axial component of the particle displacement and (b) transverse component.

Table 2
Wavenumbers $\bar{\kappa}_m$ of the propagating modes in the expansion of the second-harmonic component ($2\bar{\omega}_a = 2.8$, $2\bar{\kappa}_a = 1.988$)

Mode	First	Second	Third
RL symmetric	2.960	1.498	0.881
RL antisymmetric	3.063	1.988	—
Symmetric	2.82	1.988	—
Antisymmetric	2.63	—	—

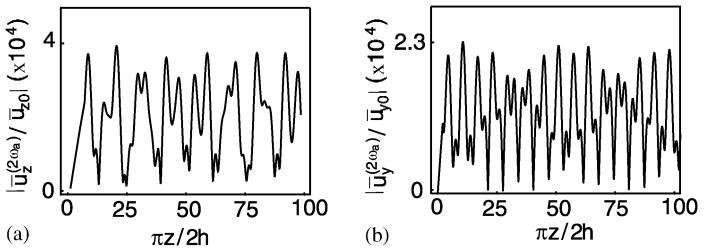

Fig. 6. Second harmonic ($2\bar{\omega}_a = 2.82$) propagating on the top of an aluminum plate, $y = h$: (a) axial component of the particle displacement and (b) transverse component.

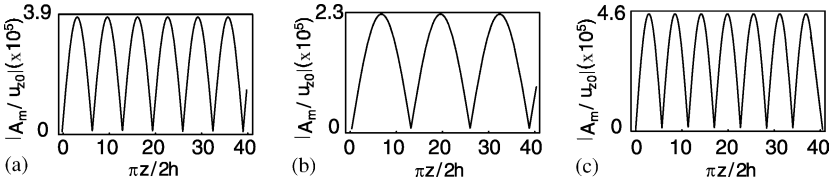

Fig. 7. Amplitudes $|A_m(z)|$ of all propagating modes comprising the solution presented in Fig. 6: (a) first symmetric mode $\bar{\kappa} = 2.96$; (b) second symmetric mode $\bar{\kappa} = 1.489$; and (c) third symmetric mode $\bar{\kappa} = 0.881$.

We can generalize this observation by saying that a primary RL mode (symmetric or antisymmetric) cannot excite SH modes (symmetric or antisymmetric) of the second-harmonic solution. However, we will see in the second example, presented in Section 4.3.2, that primary SH modes can excite RL modes in the expansion of the second-harmonic solution.

No power flux from the primary wave to the antisymmetric RL mode occurs because the forcing terms $\bar{\mathbf{S}}^{2\omega_a}$ and $\bar{\mathbf{f}}^{2\omega_a}$, which have a quadratic term in $\mathbf{u}$, are also symmetric with respect to the plane $y = 0$, and consequently using parity symmetry in y we can conclude that f_m^{vol} and f_m^{surf} are zero. Following this same reasoning, we can say that in general a symmetric (antisymmetric) primary RL mode does not excite antisymmetric (symmetric) secondary RL modes used in the expansion of the second-harmonic solution.

In Fig. 6 are plotted the magnitudes of the second-harmonic components along the surface of the plate ($y = h$), normalized by the amplitude of the primary wave at that same location. The magnitudes of the axial and transverse components of the dimensionless displacement of the primary wave (first symmetric RL mode) evaluated on the surface of the plate ($y = h$) are $\bar{u}_{z0} = 1.0 \times 10^{-9}$ and $\bar{u}_{y0} = 1.0 \times 10^{-9}$, respectively. Fig. 7 shows the magnitudes of the non-zero modal

amplitudes $\bar{A}_m(z)$ for the propagating modes used to plot Fig. 6. These amplitudes oscillate with spatial periodicities given by

$$\bar{L}_m = \left| \frac{2\pi}{\bar{\kappa}_m - 2\bar{\kappa}} \right|, \tag{71}$$

where $\bar{L}_m = \pi L_m/2h$ is the dimensionless dispersion length that follows from Eqs. (43) for propagating modes.

Therefore, despite of the existence of phase matching between the primary wave (first symmetric RL mode) and two modes at the second-harmonic frequency (second antisymmetric RL and second symmetric SH modes), internal resonance does not occur, and consequently the second-harmonic component propagates with bounded amplitude because only non-resonant modes have non-zero modal amplitudes $A_m(z)$.

4.3.2. Example 2: second harmonic, resonance

Here, a monofrequency source at frequency $\bar{\omega}_a = 1.15$ excites the first antisymmetric SH mode ($\bar{\kappa}_a = 0.568$). The modes used in the second-harmonic ($2\bar{\omega}_a = 2.3, 2\bar{\kappa}_a = 1.136$) expansion are presented in Table 3.

Phase matching occurs between the second symmetric RL and the second symmetric SH modes. The axial and transverse components of the vectors $\bar{\mathbf{f}}^{2\omega_a}$ and $\bar{\mathbf{S}}^{2\omega_a} \cdot \mathbf{n}_y$ are even and odd functions, respectively, with respect to the plane $y = 0$. The x components of $\bar{\mathbf{f}}^{2\omega_a}$ and $\bar{\mathbf{S}}^{2\omega_a} \cdot \mathbf{n}_y$ are zero, since for a SH mode $u_y = u_z = 0$ and $u_x = u_x(y, z)$. In Fig. 8 are plotted the components of the vector $\bar{\mathbf{f}}^{2\omega_a}$ and in Fig. 9 are plotted the components of the vector $\bar{\mathbf{S}}^{2\omega_a} \cdot \mathbf{n}_y$. No power is transferred from the primary wave to the second symmetric SH modes used in the expansion of the second-harmonic solution, and consequently internal resonance does not occur. By using the same ideas, we can generalize this observation by saying that a primary wave in the SH mode, which can be either symmetric or antisymmetric, cannot generate any resonant SH mode at the second harmonic.

The power flux to the second symmetric RL mode is non-zero and hence this mode is responsible for the internal resonance. In Fig. 10 is plotted the particle displacement of the second harmonic along the surface of the plate and normalized by the magnitude of the primary wave ($\bar{u}_{x0} = 1.0 \times 10^{-3}$). To plot Figs. 10(a) and (b) we used only non-resonant propagating modes in the expansion, and to plot Figs. 10(c) and (d) we used only the resonant mode.

Table 3
Wavenumbers $\bar{\kappa}_m$ of the propagating modes used in the expansion of the second-harmonic component ($2\bar{\omega}_a = 2.3$, $2\bar{\kappa}_a = 1.136$)

Mode	First	Second	Third
RL symmetric	2.325	1.136	0.368
RL antisymmetric	2.525	1.350	
SH symmetric	2.3	1.136	—
SH antisymmetric	2.071	—	—

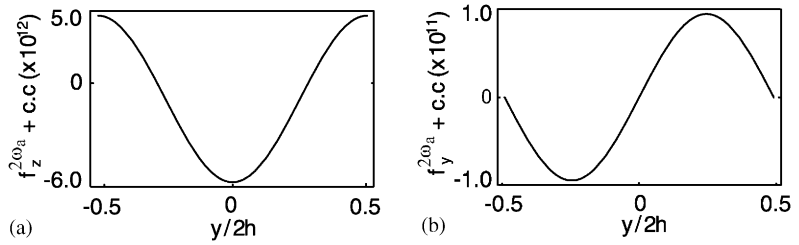

Fig. 8. Vector $\bar{\mathbf{f}}^{2\omega_a}$ for a monofrequency source that excites the first antisymmetric SH mode at frequency $\bar{\omega}_a = 1.15$: (a) axial component $\bar{f}^{2\omega_a}$ and (b) transverse component $\bar{f}_y^{2\omega_a}$.

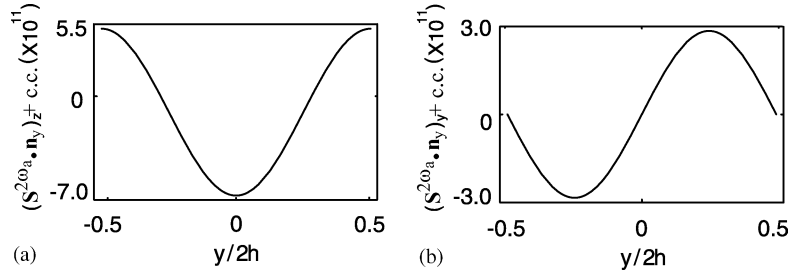

Fig. 9. Vector $\bar{\mathbf{S}}^{2\omega_a} \cdot \mathbf{n}_y$ for the first antisymmetric SH mode at primary frequency $\bar{\omega}_a = 1.15$: (a) axial component $(\bar{\mathbf{S}}^{2\omega_a} \cdot \mathbf{n}_y)_z$ and (b) transverse component $(\bar{\mathbf{S}}^{2\omega_a} \cdot \mathbf{n}_y)_y$.

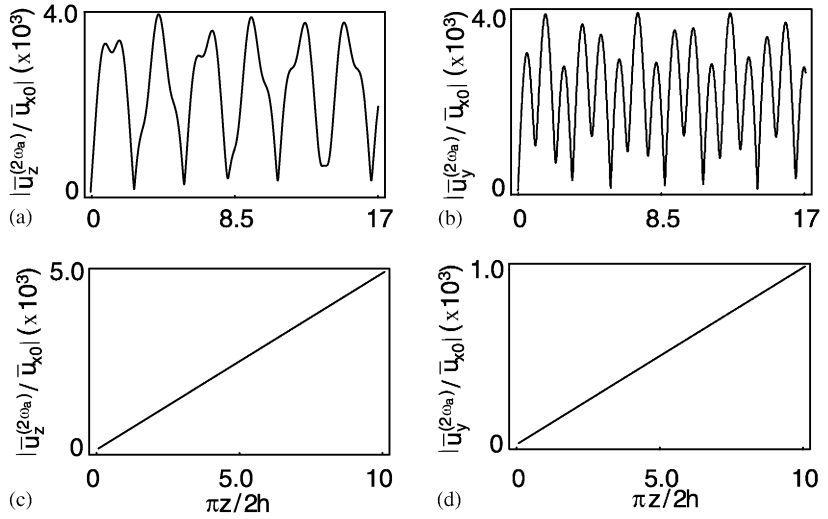

Fig. 10. Particle displacement of the second-harmonic component ($2\bar{\omega}_a = 2.3$) at the top ($y = h$) of the aluminum plate, normalized by the magnitude of the primary wave $\bar{u}_{x0} = 1.0 \times 10^{-3}$ at the same location. The magnitudes of the second harmonic using only non-resonant propagating modes in the expansion: (a) axial component and (b) transverse component. The magnitudes of the second harmonic using only the resonant mode in the expansion: (c) axial component and (d) transverse component.

From Fig. 10 we can say that the resonant mode has an amplitude of the same order as that of the other propagating modes at $\pi z_1/2h = 10$. From Fig. 10, the magnitude of the transverse component of the resonant mode is of same order as that of the primary solution when $z_2 \approx (2h/\pi) = 10^4$. For example, for a plate with thickness $2h = 1$ cm, we have $f_a = 1.1$ MHz and $u_{x0} = 3.18 \times 10^{-6}$ m, and therefore we obtain $z_1 = 0.3$ m and $z_2 = 30$ m in Eq. (48).

4.3.3. Example 3: difference frequency, resonance

For the third example, the difference-frequency component of a bifrequency source is analyzed. The source excites the first antisymmetric RL mode at frequency $\bar{\omega}_a = 4.54$ ($\bar{\kappa}_a = 4.873$), and the first symmetric RL mode at frequency $\bar{\omega}_b = 2.76$ ($\bar{\kappa}_b = 2.879$). The magnitudes of the axial and transverse components evaluated on the surface $y = h$ for the first symmetric RL mode are $\bar{u}_{z0} = 1.0 \times 10^{-5}$ and $\bar{u}_{y0} = 1.0 \times 10^{-5}$, respectively, and for the first antisymmetric RL mode they are $\bar{u}_{z0} = 1.0 \times 10^{-5}$ and $\bar{u}_{y0} = 1.0 \times 10^{-5}$, respectively. In this example, we present a case where internal resonance occurs.

Four components appear due to the non-linearity: the two second-harmonic components, and the sum- and difference-frequency components. The propagating modes used in the expansion of the second harmonics [$(2\bar{\omega}_a = 9.08,\ 2\bar{\kappa}_a = 9.746)$, $(2\bar{\omega}_b = 5.52,\ 2\bar{\kappa}_b = 5.578)$], and of the sum frequency ($\bar{\omega}_+ = 7.3,\ \bar{\kappa}_a + \bar{\kappa}_b = 7.752$) are presented in Tables 4–6. Since phase matching does not occur for any of these components, they travel only as bounded oscillations.

The propagating modes used in the expansion of the difference-frequency component ($\bar{\omega}_- = 1.78,\ \bar{\kappa}_a - \bar{\kappa}_b = 1.994$) are presented in Table 7. Note that there exists phase matching with the first antisymmetric RL mode, i.e., $\kappa_a - \kappa_b = \kappa_m$ at the difference frequency, where the subscript m stands for the first antisymmetric RL mode.

Since the axial and transverse components of the vectors $\bar{\mathbf{f}}^-$ (Fig. 11) and $\bar{\mathbf{S}}^-$ (Fig. 12) are odd and even functions, respectively, with respect to the plane $y = 0$, Eqs. (35) and (36) are non-zero for antisymmetric RL modes. Therefore the power flux from the bifrequency primary wave to the first antisymmetric RL mode at the difference frequency is non-zero, and internal resonance occurs.

In Fig. 13 are plotted the components of the particle displacement at the difference frequency along the surface of the plate and normalized by the sum of the magnitudes of the primary waves. To plot Figs. 13(a) and (b) we used only non-resonant propagating modes in the expansion, and to plot Figs. 13(c) and (d) we used only the resonant mode. It is observed that at $\pi z_1/2h \approx 2$ the amplitude of the resonant and of the non-resonant modes are of the same order. Therefore the resonant component dominates for $z \gg z_1 = 4h/\pi$. For example, for a plate with thickness $2h = 1$ cm we have $f_a = 0.7$ MHz and $f_b = 0.4$ MHz. The amplitudes of the transverse components

Table 4
Wavenumber $\bar{\kappa}$ of the propagating modes used in the expansion of the second-harmonic component ($2\bar{\omega}_a = 9.08$; $2\bar{\kappa}_a = 9.746$)

Mode	First	Second	Third	Fourth	Fifth	Sixth	Seventh	Eighth
RL symmetric	9.728	8.711	7.648	5.82	4.45	4.11	3.17	—
RL antisymmetric	9.728	8.986	8.268	6.826	4.95	4.03	2.42	1.00
SH symmetric	9.08	8.857	8.151	6.811	6.81	4.29	—	—
SH antisymmetric	9.024	8.57	7.579	5.783	1.20	—	—	—

Table 5
Wavenumbers $\bar{\kappa}_m$ of the propagating modes used in the expansion of the second-harmonic component ($2\bar{\omega}_b = 5.52$; $2\bar{\kappa}_b = 5.758$)

Mode	First	Second	Third	Fourth	Fifth
RL symmetric	5.918	5.293	3.806	2.470	1.575
RL antisymmetric	5.911	4.711	3.025	2.520	—
SH symmetric	5.52	5.51	3.804	—	—
SH antisymmetric	5.42	4.634	2.338	—	—

Table 6
Dimensionless wavenumbers $\bar{\kappa}_m$ of the propagating modes used in the expansion of the sum-frequency component ($\bar{\omega}_+ = 7.3$; $\bar{\kappa}_a + \bar{\kappa}_b = 7.752$)

Mode	First	Second	Third	Fourth	Fifth	Sixth
RL symmetric	7.821	7.1637	6.178	4.350	3.179	2.049
RL antisymmetric	7.821	6.786	5.321	3.728	3.375	2.001
SH symmetric	7.3	7.02	6.106	4.158	—	—
SH antisymmetric	7.231	6.655	5.3188	2.071	—	—

Table 7
Wavenumbers $\bar{\kappa}_m$ of the propagating modes used in the expansion of the difference-frequency component ($\bar{\omega}_- = 1.78$; $\bar{\kappa}_a - \bar{\kappa}_b = 1.994$)

Mode	First	Second
RL symmetric	1.606	—
RL antisymmetric	1.994	0.879
SH symmetric	1.78	—
SH antisymmetric	1.472	—

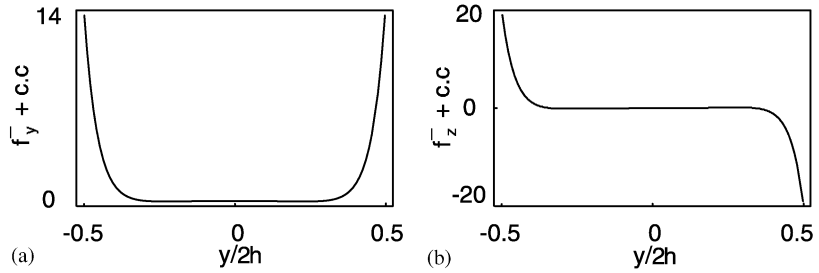

Fig. 11. Vector $\mathbf{f}^-$ for a bifrequency source that excites the first antisymmetric RL mode at frequency $\bar{\omega}_a = 4.54$ and first symmetric RL mode at frequency $\bar{\omega}_b = 2.76$: (a) transverse component f_y^- and (b) axial component f_z^-.

measured on the surface are $u_{y0} = 3 \times 10^{-9}$ m for the first symmetric RL mode and $u_{y0} = 3 \times 10^{-9}$ m for the first antisymmetric RL mode. We obtain $z_1 = 0.006$ m and $z_2 = 6.4$ m in Eq. (48). Also, at 1 m from the source we have for the transverse component of the particle displacement of the difference-frequency $|u_y^{(-)}| = 1.0 \times 19^{-9}$ m.

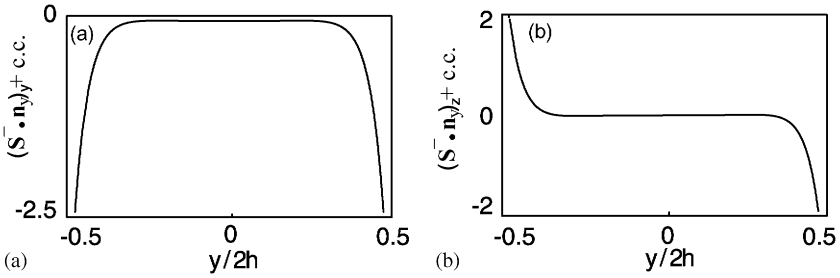

Fig. 12. Vector $(\mathbf{S}^{-} \cdot \mathbf{n}_y)$ for a bifrequency source that excites the first antisymmetric RL mode at frequency $\bar{\omega}_a = 4.54$ and first symmetric RL mode at frequency $\bar{\omega}_b = 2.76$: (a) transverse component $(\mathbf{S}^{-} \cdot \mathbf{n}_y)_y$ and (b) axial component $(\mathbf{S}^{-} \cdot \mathbf{n}_y)_z$.

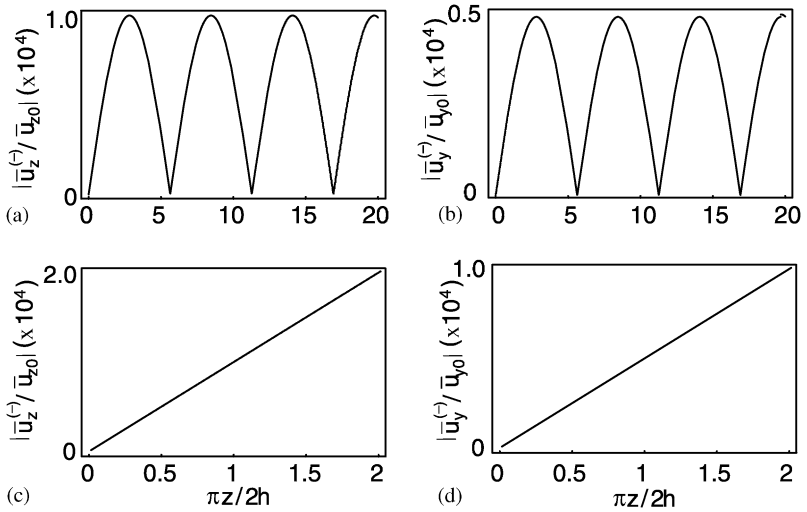

Fig. 13. Particle displacement of the difference-frequency component ($\bar{\omega}_{-} = 1.78$) at the top ($y = h$) of the aluminum plate: magnitude of difference-frequency component with only non-resonant propagating modes used in the expansion: (a) axial component and (b) transverse component. Magnitude of difference-frequency component with only the resonant mode used in the expansion: (c) axial component and (d) transverse component. The dimensionless amplitude $\bar{u}_{y0} = 2.0 \times 10^{-5}$ is the sum of the amplitude of the primary waves.

5. Summary

Harmonic generation in elastic isotropic plates was investigated in this paper. Since the associated boundary value problem consists of equations that are mathematically similar to those for forced linear waveguides, the method developed by Auld [23] was used here to obtain the solution for harmonic generation. The forcing functions applied in the volume and on the surface are found by substituting the primary wave solution in the non-linear terms of the equation of motion and in the stress-free boundary condition.

In this method, the source condition is applied to each of the coefficients in the expansion of the second-order solution, and hence it is satisfied independently of the number of modes used in the expansion. The boundary conditions are satisfied for each coefficient via simple integrals. The

method allows us to quantify the influence of the primary solution in each mode in the expansion of the secondary solution. Also with this method, the two conditions for internal resonance appear naturally in the solution: (1) phase matching; (2) non-zero power transfer from the primary wave to the modes used in the expansion of the secondary solution.

When internal resonance occurs there exists an interval $[z_1, z_2]$ where only the resonant mode is needed in the expansion of the secondary solution. The lower limit z_1 is the distance where the magnitude of the resonant mode is of the same order of the magnitude of the sum of all non-resonant modes. The upper limit z_2 is the distance where the magnitude of the resonant mode equals the magnitude of the primary wave. Here we used only propagating modes to estimate z_1 and z_2. Due to the mechanism of dissipation, which was disregarded here, the actual values of z_1 and z_2 are different from those estimated. However, for materials with small coefficients of attenuation, such as metals at room temperature, we expect a small difference between the actual and the estimated values of z_1 and z_2.

The power transferred from the primary wave to the modes in the expansion of the secondary wave was evaluated. Explanation of zero power transfer was provided on the basis of symmetry of the modes with respect to the middle plane of the plate.

Acknowledgements

The authors wish to acknowledge the support of the National Science Foundation, Mechanics and Materials Program, and the Conselho Nacional de Desenvolvimento Científico e Tecnológico (CNPq) of Brazil.

References

[1] D.S. Drumheller, Introduction to Wave Propagation in Nonlinear Fluids and Solids, Cambridge University Press, New York, 1998.
[2] A.N. Norris, Finite-amplitude waves in solids, in: M.F. Hamilton, D.T. Blackstock (Eds.), Nonlinear Acoustics, Academic Press, New York, 1998 (Chapter 9).
[3] M.F. Hamilton, Yu.A. Il'inskii, E.A. Zabolotskaya, Nonlinear surface acoustic waves, in: W. Lauterborn, T. Kurz (Eds.), Proceedings of the 15th International Symposium on Nonlinear Acoustics: Nonlinear Acoustics at the Turn of the Millenium, Göttingen, Germany, September 1999, American Institute of Physics, New York, 2000, pp. 55–64.
[4] A.P. Mayer, Surface acoustic waves in nonlinear elastic media, Physical Report 256 (1995) 237–366.
[5] D.E. Bray, R.K. Stanley, Nondestructive Evaluation. A Toll in Design, Manufacturing and Service, McGraw-Hill, New York, 1989.
[6] L.W. Schmerr Jr., Fundamentals of Ultrasonic Nondestructive Evaluation. A Modeling Approach, Plenum Press, New York, 1998.
[7] D.E. Chimenti, Guided waves in plates and their use in materials characterization, Applied Mechanics Reviews 50 (1997) 247–284.
[8] P. Cawley, D.N. Alleyne, The use of Lamb waves for long range inspection of large structures, Ultrasonics 34 (1996) 287–290.
[9] H. Kwun, K.A. Bartels, Experimental observation of elastic-wave dispersion in bounded solids of various configurations, Journal of the Acoustical Society of America 99 (1996) 962–968.

[10] M.J.S. Lowe, D.N. Alleyne, P. Cawley, Defect detection in pipes using guided waves, Ultrasonics 36 (1998) 147–154.
[11] G.E. Dace, R.B. Thompson, L.J.H. Brash, Nonlinear acoustics, a technique to determine microstructural changes in materials, in: D.O. Thompson, D.E. Chimenti (Eds.), Review of Progress in Quantitative Nondestructive Evaluation, Vol. 10B, Plenum Press, New York, 1991, pp. 1685–1692.
[12] A.M. Sutin, D.M. Donskoy, Nonlinear vibro-acoustic nondestructive testing technique, in: J.R.E. Green (Ed.), Nondestructive Characterization of Material VIII, Plenum Press, New York, 1998.
[13] Y. Zheng, R.G. Maev, I.Y. Solodov, Nonlinear acoustic application for material characterization: a review, Canadian Journal of Physics 77 (1999) 927–967.
[14] A.M. Sutin, D.M. Donskoy, Vibro-acoustic modulation nondestructive evaluation technique, SPIE 3397 (1998) 226–237.
[15] V.Y. Zaitsev, A.M. Sutin, I.Y. Belyaeva, V.E. Nazarov, Nonlinear interaction of acoustical waves due to cracks and its possible usage for crack detection, Journal of Vibration and Control 1 (1995) 335–344.
[16] A.E. Ekimov, I.N. Didenkulov, V.V. Kazakov, Modulation of torsional waves in a rod with a crack, Journal of the Acoustical Society of America 106 (1999) 1289–1292.
[17] K.E.A. Van Den Abeele, P.A. Johnson, A. Sutin, Nonlinear elastic wave spectroscopy (NEWS) techniques to discern material damage, Part I: nonlinear wave modulation spectroscopy (NWMS), Research in Non-destructive Evaluation 12 (2000) 17–30.
[18] K.E.A. Van Den Abeele, J. Carmeliet, J.A. Ten Cate, P.A. Johnson, Nonlinear elastic wave spectroscopy (NEWS) techniques to discern material damage, Part II: single-mode nonlinear resonance acoustic spectroscopy, Research in Nondestructive Evaluation 12 (2000) 31–42.
[19] A.M. Samsonov, Nonlinear acoustic strains waves in elastic waveguides, in: J. Engelbrecht (Ed.), Nonlinear waves in solids, Springer, New York, 1994 (Chapter 6).
[20] M. Deng, Second-harmonic properties of horizontally polarized shear modes, Japan Journal of Applied Physics 35 (1996) 4004–4010.
[21] M. Deng, Cumulative second-harmonic generation accompanying nonlinear shear horizontal mode propagation in a solid plate, Journal of Applied Physics 84 (1998) 3500–3505.
[22] M. Deng, Cumulative second-harmonic generation of Lamb mode propagation in a solid plate, Journal of Applied Physics 85 (1999) 3051–3058.
[23] B.A. Auld, Acoustic Fields and Waves in Solids, Vols. I and II, Wiley, London, 1973.
[24] E.Yu. Knight, M.F. Hamilton, Yu.A. Il'inskii, E.A. Zabolotskaya, General theory for the spectral evolution of nonlinear Rayleigh waves, Journal of the Acoustical Society of America 102 (1997) 1402–1417.
[25] W.J.N. de Lima, Harmonic Generation in Isotropic Elastic Waveguides, Ph.D. Dissertation, The University of Texas at Austin, 2000.
[26] Z.A. Gol'dberg, Interaction of plane longitudinal and transverse elastic waves, Soviet Physics-Acoustics 6 (1960) 306–310.
[27] L.D. Landau, E.M. Lifshitz, Theory of Elasticity, 3rd Edition, Pergamon Press, New York, 1986.
[28] K.F. Graff, Wave Motion in Elastic Solids, Dover Publications, New York, 1991.
[29] Y. Pao, R.K. Kaul, R.D. Mindlin, Waves and vibrations in isotropic and anisotropic plates, in: G. Herrmann (Ed.), Applied mechanics, Pergamon Press, New York, 1974, pp. 149–195.
[30] A.H. Nayfeh, D.T. Mook, Nonlinear Oscilations, Wiley, London, 1979.
[31] B.J. Landsberger, Second Harmonic Generation in Sound Beams Reflected from and Transmitted through Immersed Elastic Solids, Ph.D. Dissertation, The University of Texas at Austin, 1997.
[32] L.E. Kinsler, A.R. Frey, A.B. Coppens, J.V. Sanders, Fundamentals of Acoustics, Wiley, New York, 1994.
[33] R.F.S. Hearmon, The third- and higher-order elastic constants, in: K.H. Hellwege, A.M. Hellwege (Eds.), Elastic, Piezoelectric, Pyroelectric, Piezooptic, Electroptic Constants, and Nonlinear Dielectric Susceptibilities of Crystals, Vol. III/11, Landolt-Börnstein, New Series, Springer, New York, 1979, pp. 109–308.